MINIREVIEW

Imaging Stem Cell Implant for Cellular-Based Therapies

ZHENGHONG LEE,*[,1] JAMES E. DENNIS,† AND STANTON L. GERSON‡

*Departments of Radiology and Biomedical Engineering, National Center for Regenerative Medicine, Case Western Reserve University, Cleveland, Ohio 44106; †Department of Orthopedics, National Center for Regenerative Medicine, Case Western Reserve University, Cleveland, Ohio 44106; ‡Division of Hematology-Oncology, National Center for Regenerative Medicine, Case Western Reserve University, Cleveland, Ohio 44106

Stem cell–based cellular therapy represents a promising outlook for regenerative medicine. Imaging techniques provide a means for noninvasive, repeated, and quantitative tracking of stem cell implant or transplant. From initial deposition to the survival, migration and differentiation of the transplant/implanted stem cells, imaging allows monitoring of the infused cells in the same live object over time. The current review briefly summarizes and compares existing imaging methods for cell labeling and imaging in animal models. Several studies performed by our group using different imaging techniques are described, with further discussion on the issues with these current imaging approaches and potential directions for future development in stem cell imaging. Exp Biol Med 233:930–940, 2008

Key words: stem cell imaging; hematopoietic stem cell; mesenchymal stem cell; bioluminescent imaging; positron emission tomography; cell-based therapy

Introduction

There is increasing evidence that adult human tissues harbor stem cells and progenitor cells that can be used for therapeutic purposes. Bone marrow contains pluripotent hematopoietic stem cells (HSCs) that continuously produce blood cells throughout our lifetime with the characteristics of self-renewal and differentiation into progenitor cells, leading to generation of all hematopoietic lineages. HSC transplantation has proven to be a life-saving therapy for diseases refractory to other treatments (1). A total of 27,902 HSC transplantations were performed from 1991–2002 in Europe for solid tumors alone (2). Although effective, this therapy remains toxic with treatment-related mortality of approximately 5% for autologous transplantation and 20–40% for allogeneic transplantation. Interventions to reduce the toxicity and make this therapy available to a larger patient population are urgently needed. HSC-based gene therapy has been an established cellular therapy for patients with hematological diseases, and it has shown great potential for the emerging field of regenerative medicine. However, the efficiency of current oncoretroviral gene transfer is limited. Two of the most problematic reasons are insertional mutagenesis and low transduction efficiency. *In vivo* drug selection has been shown to be effective in enriching transduced cells, thus enhancing transgene expression. The effective selection using MGMT (P140K) gene has been shown in numerous studies. To monitor this dynamic selection process as well as to follow HSC transplant in general, noninvasive and longitudinal tracking methods are much needed.

In addition to HSCs, bone marrow also contains progenitor cells that can differentiate into multiple mesenchymal phenotypes (3, 4). It has been proposed that the mesenchymal progenitors of bone marrow are part of a mesenchymal lineage (5) analogous to that described for

This work was supported in part by DOE (DE-FG02-03ER63597 to Z Lee), NIH R21 (EB001847 to Z Lee), NIH R24 (CA110943 to JL Duerk), NIH R01(AR49785 to JE Dennis), NIH R01 (CA073062 to SL Gerson), and JLab sub-contract (SURA-04-Q011).

[1] To whom correspondence should be addressed at Departments of Radiology and Biomedical Engineering, National Center for Regenerative Medicine, Case Western Reserve University, 11100 Euclid Avenue, Cleveland, Ohio 44106. E-mail: Zxl11@case.edu

DOI: 10.3181/0709-MR-234
1535-3702/08/2338-0930$15.00

hematopoiesis and that the multipotential progenitors in marrow may be mesenchymal stem cells (MSCs), or multipotent marrow *s*tromal cells (MSCs). MSCs are pluripotent adult stem cells found in adult donor bone marrow that can differentiate into bone, cartilage, and adipose tissue (4–6). Autologous and allogeneic transplantation of hMSCs has been reported to have positive effects for the treatment of several human diseases and conditions. For example, in bone marrow transplant recipients, intravenously (i.v.)-administered MSCs have been reported to promote engraftment of hematopoietic lineages in cancer patients receiving high dose chemotherapy (7) and ameliorate graft versus host disease (GVHD) (8, 9). Furthermore, i.v.-administered hMSCs have been shown to home to neoplasms *in vivo*, and thus have the potential to serve as vehicles for the delivery of anticancer therapies (10). Finally, hMSCs injected in the setting of myocardial infarction and stroke have been shown to improve postischemic regeneration and function (11, 12). These studies indicate that MSCs can be engineered to secrete functional cytokines and used for hematopoietic support *in vivo*. Most of the proposed MSC therapies entail the local application of MSCs. However, systemic delivery of MSCs with subsequent organ engraftment would allow clinical use in a variety of settings such as treatment of osteopenia, myocardial infarction, repair of bone metastasis, and facilitation of hematopoietic engraftment. The promise of MSC therapeutics mandates research leading to a better understanding of the long-term fate and trafficking of transplanted MSCs *in vivo*. Previously, the majority of such research relied on *ex vivo* labeling MSCs by various methods, performing transplants, and sacrificing animals at serial post-transplant time points to look for histological evidence of MSC fate. This methodology has the obvious drawback of making the understanding of the longitudinal fate of the transplant within a given recipient impossible. A noninvasive, repeated, and quantitative method to monitor allogeneic hMSC transplants *in vivo* would be highly desirable.

Our imaging work is mostly with HSCs and MSCs (including related multipotent adult progenitor cells or MAPC, etc.) although there are other types stem cells and progenitors, most noticeably, the embryonic stem cells (ESCs) that are pluripotent. We and others realize that high dose anticancer therapy and HSC transplantation is a curative therapy for a number of hematological malignancies and has been investigated in the management of solid tumors as mentioned above. We have focused on improving transplantation outcome by improving hematopoietic engraftment and reducing complications such as GVHD. We have conducted preclinical and clinical studies with a novel marrow-derived stem cell, using the MSCs as facilitator cells to improve HSC engraftment and overcome immune complications of transplantation. We also developed drug resistance gene therapy of HSCs and developed models of bone marrow protection from chemotherapy and selective expansion of donor cells without using high dose therapy. Despite considerable progress in the therapeutic uses of HSCs and MSCs, little is understood about the biology of stem cell engraftment, especially the dynamic processes of homing, tissue migration, engraftment, and expansion. To elucidate *in vivo* behavior of these cells, we set out to develop sensitive and quantitative imaging technologies, as reported in this review, to measure stem cell distribution, survival, engraftment, and proliferation. The long-term goal is to use *in vivo* imaging to monitor stem cell engraftment and interaction with the host microenvironment to improve the therapeutic potential of stem cell infusion and organ implantation for the treatment of cancer and other diseases. Quantitative and sensitive *in vivo* imaging methods for stem cell tracking are also critical to the optimization of therapeutic potential of stem cells through measuring the impact of various cellular and genetic interventions on the *in vivo* distribution and survival of the stem cells.

Stem Cell Imaging Techniques

Overview. Recently, noninvasive, imaging-based monitoring methods have been developed to track stem cell transplants by labeling the cells. The goal is to track the disposition, distribution, and migration of stem cells once introduced into the model organism. The ability to track the location of cells will allow several questions to be answered: 1) If injected through the vein where do these cells go? 2) If implanted do cells remain at the site of implantation or do they migrate? 3) Once in target locations, how do they interact with their microenvironment? 4) Can transplanted cells differentiate into desired tissues?

Basically, there are two methods to label the cells: direct and indirect. Direct labeling is to introduce a marker into or onto the cells before transplant/implant that is stably incorporated or attached to the cells. Examples include labeling with iron oxide particles such as the super paramagnetic iron oxides (SPIO) or perfluoropolyether or perfluorocarbon nano-beacons for Magnetic Resonance (MR) imaging (13–15), which is extended from cancer cell labeling, or with [^{18}F]-HFB or [^{18}F]-FDG for Positron Emission Tomography (PET) imaging (16, 17), or with [^{111}In]-Oxine or [^{111}In]-Tropolone for gamma scintigraphic imaging (18–20), which is adapted from traditional labeling of blood cells such as leukocytes for use in infection/inflammation imaging in Nuclear Medicine (21–23). Direct labeling for MR imaging allows the depiction of initial deposition of the implanted stem cells, but the imaging signal diminishes or becomes undetectable with cell division. A confounding factor with this type of labeling and imaging is that dead cells still generate signals for days before macrophage clearance of cellular debris. Recent data confirm that a significant number of MSCs implanted into an infracted heart undergo apoptosis (24), and direct labeling would show the location of the dead or dying cells. Direct labeling of cells with radionuclides can only

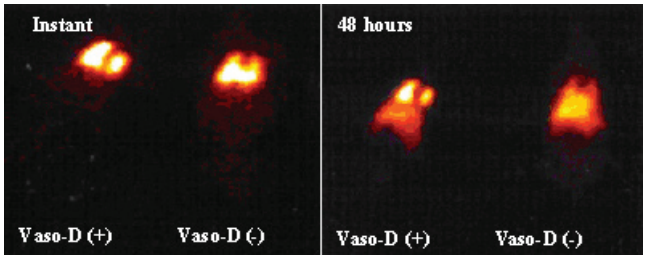

Figure 1. Gamma scintigraphic scans of two rats at 15 minutes and 48 hours after injection of indium^{111}-oxine labeled MSCs (IV) with (D+) or without (D–) vasodilator.

determine short-term circulation and homing properties of infused stem cells because the imaging signal decreases with radio-decay, or becomes more diffused with cell division and cell dispersion.

Indirect labeling relies on the expression of imaging reporter genes transduced into the cells before transplantation, which are then visualized upon injection of appropriate probes or substrates. Examples of this approach include labeling the cells with firefly luciferase (*fluc*) for bioluminescent imaging (BLI), where visible light is emitted from the biochemical reaction of luciferase enzyme with its substrate; thymidine kinase of herpes simplex type one virus (HSV1-*tk*, or *tk*) for PET imaging (25–27), where a pair of high energy gamma photons generated from the radio-decay of radiolabeled substrate of HSV1-TK are detected to form an image; and transferrin receptor (*TfR*) that can be used for nuclear or MR imaging (28). The reporters for use in optical imaging such as *fluc* (for BLI) or fluorescent proteins (GFP, RFP, etc., for fluorescent imaging) are modified from traditional lab/bench approaches for cell (including stem cell) related research. *fluc* brings high sensitivity with BLI on small animal models but cannot be easily translated into clinical uses due to constraints of tissue penetration of visible light photons. However, the other reporter genes such as the *tk* gene allow quantitative PET imaging and have the potential for translation into a clinical setting, because high energy gamma photons from positron decay can penetrate deep tissues and organs. Overall, reporter gene-based imaging offers unique capabilities for noninvasive and longitudinal measurements, which can minimize the number of research animals required by obviating the need to sacrifice animals at multiple time points.

Descriptions and discussions about different imaging techniques and modalities are beyond the scope of this review. However, nonimaging readers can consult several references that cover these different modalities (29–31). In addition, there are recent reviews on using individual imaging modalities such as using MRI for stem cell imaging (32, 33), or specific/disease-based reviews such as imaging stem cell implant for cardiac applications (34). We have conducted imaging studies that include mainly BLI and PET experiments for general purpose stem cell imaging and are reported in the following sections.

Table 1. Biodistribution Data from 48 Hrs After Transplant Used to Validate Image Data

Organ	After vasodilator (%)	No vasodilator (%)	
Liver	29.16 (6.25)	25.47 (5.82)	
Lung	15.39 (4.62)	24.30 (5.66)	$P = 0.013$
Bone	1.24 (0.42)	0.46 (0.21)	$P = 0.0023$
Kidney	4.74 (1.25)	3.96 (1.22)	
Spleen	1.51 (0.33)	1.43 (0.26)	

Direct Labeling. As an initial attempt to determine short-term circulatory and homing properties of MSCs, we conducted planar gamma scintigraphic imaging of the rats infused with [^{111}In]-Oxine–labeled MSCs (19). The MSCs were isolated from 3–4-month-old Fisher F-344 rats and cultured as previously described (35). For [^{111}In]-Oxine labeling, the MSCs were transferred to a local pharmacy of Mallinckrodt, Inc. (Independence, OH) approximately 5 hrs before the scheduled infusion. Different routes of infusion were tested. Fifteen planar whole body images were acquired with one-min intervals using a clinical scanner, the E.CAM (Siemens Medical Systems, Inc., Hoffman Estates, IL) immediately after infusion. The initial results of the labeled MSC infusion with and without vasodilator therapy showed pulmonary entrapment (Figure 1). In this experiment, vasodilator (sodium nitroprusside, 1.0 mg/kg body mass) was injected prior to MSCs infusion to promote vasodilatation and pulmonary shunts. The image on the right shows the same rat at 48 hrs postinfusion. To validate the imaging data, organs (lungs, liver, kidneys, spleen, and long bones with marrow) of the rats were harvested, weighed, and the radioactivity quantified by a 1282 CompuGamma (Wallac, Inc., Gaithersburg, MD). The results are expressed as a percentage of injected dose (mean and standard deviation) as shown in Table 1. The initial distribution of infused MSCs could only be acquired over a limited time period due mainly to the half-life of the radionuclide (2.8 days for ^{111}In), which is the primary limiting factor for most direct labeling. While being able to quantify the number of injected cells found in different tissues is an advantage of this system, there is a need to monitor stem cell transplant over a much longer time span in order to study homing and engraftment, which clearly cannot be done with ^{111}In labeling.

BLI with *fluc*. The tremendous advantage of BLI has been increasingly recognized over the past few years. More and more researchers are using BLI to monitor and understand dynamic biological processes in real-time. *In vitro* assays using a luminometer to measure promoter activity, gene expression, or ATP level have existed for a long time. The most studied and widely used luminescent protein is firefly (*Photinus pyralis*) luciferase (*fluc*). *fluc* is a 61-kDa monomeric protein, which reacts with its substrate D-luciferin in the presence of oxygen, Mg^{2+}, and ATP to release green light with peak wavelength at 562 nm (36).

Figure 2. P140K-MGMT-2A-fluc lenti-vector with MND promoter and 2A cleavage site.

BLI with *fluc* has become a valuable imaging modality for monitoring gene expression, protein and protein interaction, viral infection, cancer growth and metastasis, treatment progress, and cell trafficking in real-time (37–43). *fluc* is also very useful as a marker for cells for studying migration *in vivo*. In transplantation models, bone marrow cells of the donors can be tagged by retroviral vectors or lentiviral vectors containing the *fluc* gene. After infusion, tagged bone marrow cells can be tracked to provide information on their homing, expansion, and engraftment. Wang et al. used lentiviral vectors to transduce human $CD34^+$ and more primitive $CD34^+CD38^-$ cells obtained from umbilical cord blood, and the transduced $CD34^+$ and $CD34^+CD38^-$ cells were infused into nonobese diabetic/severe combined immunodeficient (NOD/SCID) mice. Bioluminescent signals were generated after 2 to 3 weeks and up to 108 days, which was consistent with short-term engraftment of $CD34^+$ cells and late-term engraftment of $CD34^+CD38^-$ cells (43). Similar experiments were conducted by Cao et al., using *fluc* transgenic mice with β-actin promoter as donor. KTLS ($Lin^-Sca\text{-}1^+c\text{-}Kit^+Thy\text{-}1^{lo}$) HSC was purified from the donor and transplanted into the irradiated recipients at different concentrations. BLI signals indicated that initial foci in the spleen and bone marrow have different kinetics, but overall BLI signal was consistent with concentration of purified HSC (44).

We experimented with *fluc* on HSCs for BLI on mouse models for enrichment of HSC transplant (45). The purpose was to monitor the impact of drug selection on the engraftment of short-term repopulating cells and its potential impact on the long-term repopulating cells. Lentiviral vector containing *fluc* (pLV-fluc) was generously provided by Dr. D. B. Kohn (Children's Hospital Los Angeles, CA) with a MND promoter, which was derived from myeloproliferative sarcoma viruses (MPSV) and has been shown to effectively promote gene expression in bone marrow cells (46). The chemo-drug resistant gene P140K MGMT and *fluc* gene were linked by the ribosomal cleavage site, 2A sequence, a sequence from foot-and-mouth disease virus, which is 19 amino acids long and has been reported to be an intraribosomal cleavage site (47, 48).

Table 2. Mixture of Transduced and Untransduced Bone Marrow Cells for Transplantation

Group	Transduced cells	Untransduced cells	% of transduced cells	Total cells transplanted
1	0	1×10^6	0	1×10^6
2	1×10^5	9×10^5	10	1×10^6
3	6×10^5	4×10^5	60	1×10^6

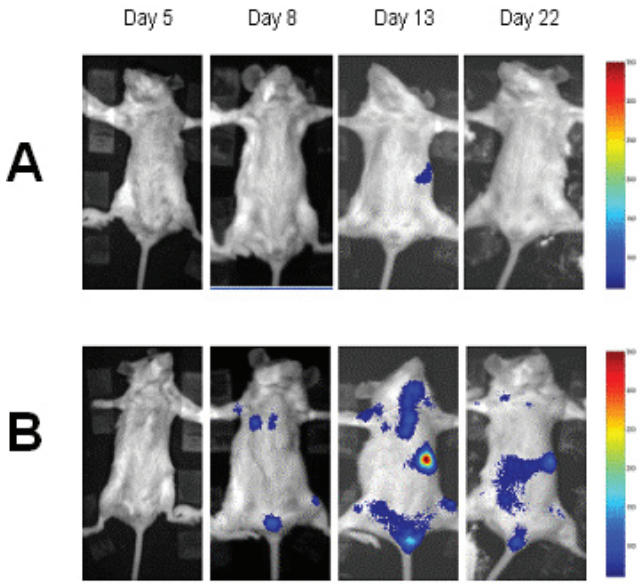

Figure 3. Imaging of P140K-MGMT-2A-fluc lenti-vector transduced BALB/c bone marrow cells infused into lethally irradiated congeneric mice with different cell numbers. (A) 1×10^5 transduced cells plus 9×10^5 untransduced cells; (B) 6×10^5 transduced cells plus 4×10^5 untransduced cells.

P140K-MGMT gene and 2A PCR product were cloned together into pLV-*fluc* with unique restriction sites, and the clones were digested and sequenced to ensure the correct orientation and in frame (Figure 2). Bone marrow cells were collected from the femur and tibia of 6–8-week-old female BALB/c mice (Jackson Laboratories) 4 days after treatment with 150 mg/kg 5-fluorouracil (5-FU). Cells were transduced with P140K MGMT-2A-*fluc* lenti-viruses at MOI of 1.4. Forty-eight hrs after transduction, cells were mixed at different percentage of transduced and untransduced cells (Table 2). Congeneric 7–8-week-old female BALB/c mice (Jackson Laboratories) were used as recipient mice and separated into two pre-transplantation conditions. Lethally irradiated recipients received 800 cGy from Cs source 1 day before transplantation, and nonmyeloablated recipients received chemo-drugs BG (30 mg/kg) and BCNU (10 mg/kg) 48 hrs before transplantation. A mixture of 1 million bone marrow cells labeled and unlabeled with *fluc* was injected through the tail vein into each recipient mouse. BLI was performed on a cooled-CCD camera IVIS 200 (Xenogen, Palo Alto, CA) at various time points. Each mouse was anesthetized and injected intraperitoneally (i.p.) with 110 mg/kg of D-luciferin (Pierce Biotechnology, Inc.) right before imaging. Image signal from each mouse was compared and pseudo-colored. Lethally irradiated recipients received no further drug treatment. BLI signal was detected in mice with larger number of reporter gene transduced cells (Figure 3B) as early as 6–8 days after transplantation. By Day 12–14, the strong signal appeared at the region of the spleen, and at other locations, especially in the bone marrow of the femur and vertebrate. By week 3, signals from the

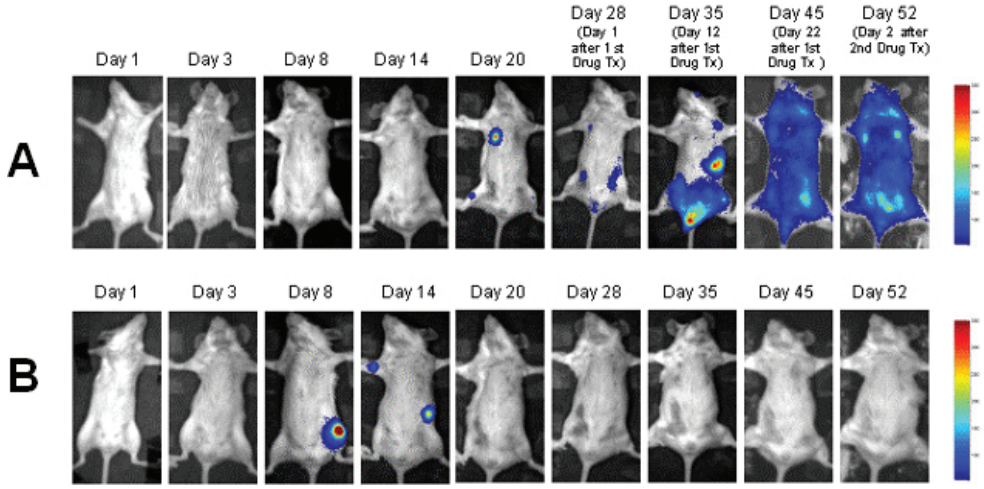

Figure 4. Pattern of clonal expansion and engraftment of P140-MGMT-2A-fluc lenti-vector transduced bone marrow cells under selection of BG + TMZ in non-myeloablated condition. (A) 1×10^5 transduced plus 9×10^5 untransduced cells injected via tail-vein, and the mouse received two sets of BG + TMZ treatments (see text); (B) 6×10^5 transduced plus 4×10^5 untransduced cells also injected via tail-vein without drug selection.

spleen remained while that from the others were reduced and even disappeared. The transgene expression level or clonal expansion from transplanted bone marrow cells appears to be a dynamic process. The progenitor cells may die off or migrate to another location over a couple of days. HSC engraftment in nonmyeloablated recipients appears to be impeded, perhaps because there is no niche for the injected cells to engraft. Introducing a selective gene into transgene and using drug selection have been proven to be a feasible approach (49). We used temozolomide (TMZ), an oral methylating agent that has been very effective against advanced cancer and brain tumor (50), and proven effective for *in vivo* selection of HSC (51). Three weeks after transplantation, nonmyeloablated recipients were treated with BG (30 mg/kg) and TMZ (80 mg/kg) for 3 consecutive days. Images were taken each week to monitor the clonal expansion of transduced HSC. Three weeks later, a second BG + TMZ treatment was administered. In one nonmyeloablated recipient, which received 6×10^5 transduced bone marrow cells without drug treatment, BLI signal was present on Days 8 and 14, but the signal disappeared afterward (Figure 4B). In another nonmyeloablated recipient with drug treatment, the signal was detected before the treatment and spread throughout the body after the treatment, indicating the strong expansion and engraftment of transduced HSC (Figure 4A). Drug selection could also have induced differentiation of transduced progenitor cells, causing the increased and spread signal. However, the engraftment pattern was more similar to the engraftment of HSC in lethally irradiated recipients. These results are encouraging for using drug selection to enhance engraftment in gene therapy.

Imaging with NIS Gene. Na^+/I^- Symporter (NIS) facilitates the accumulation of iodide by thyroid follicular cells to concentrations 20–40-fold over the plasma levels. Human NIS is expressed in thyroid, salivary, and lactating mammary glands as well as gastric mucosa. NIS is not expressed elsewhere and is thus a good reporter gene for imaging. The radio-probes for NIS are simply the radioiodide, I-125, I-123, and I-131, or technetium [^{99m}Tc]-pertechnetate ([^{99m}Tc]-TcO_4^-). All of these radionuclides are readily available in almost all Nuclear Medicine clinics and no radio synthesis is required. Both radioiodide and [^{99m}Tc]-TcO_4^- are well understood for their metabolism and clearance in the body. The imaging potential of NIS has been shown *in vitro* (52). Tumor xenografts expressing exogenous NIS have been imaged *in vivo* (53). Recent mouse scintigraphic studies have thoroughly documented pharmacodynamics of radioiodide and pertechnetate in the target organs and surrounding tissues/organs (54). The NIS reporter gene has been used to monitor neural stem cells (NSCs) (55).

We used NIS as a reporter gene specifically for imaging of MSC homing and engraftment on a mouse model with radioiodide or pertechnetate. A second generation lentiviral vector was used to optimize the transduction of MSCs. A 2.5kb fragment containing human NIS was isolated from 7.9kb pcDNA3 plasmid (gift from Sissy Jhiang, Ohio State University) by restriction digestion and then ligated into the 8.65kb wpt vector using the Fast Link DNA Ligation Kit from Epicenter. The lentiviral vector wpt.hNIS supernatant was added to MSCs and incubated for 6 hrs for 2 consecutive days. After hNIS transduction, radioiodide uptake in NIS-MSCs was determined. The iodide (uptake) counts were proportional to the number of NIS-transduced MSCs (56). The perchlorate inhibition assay was also performed showing complete inhibition of I-123 uptake and validated the specificity of NIS mediated iodide uptake in the transduced cells (56).

Two imaging experiments were conducted using NOD-SCID mice as recipients of human MSC transplant/implant (57). These NOD-SCID mice are deficient in B, T, and NK

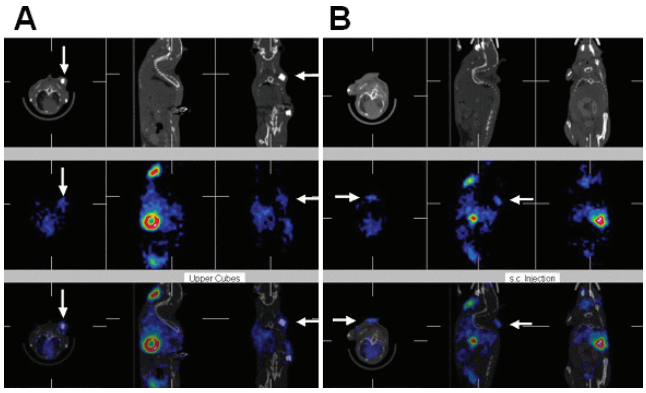

Figure 5. Imaging stem cell implant with NIS gene as the reporter. Overlays of CT and SPECT images with the arrows pointing to the upper left cube (A), which is loaded with NIS-transduced MSCs; to the s.c. injection site (B) with the same NIS-transduced MSCs. The thyroid/salivary glands and the stomach (gastric mucosa) have high uptake in both (A) and (B) due to endogenous NIS expression.

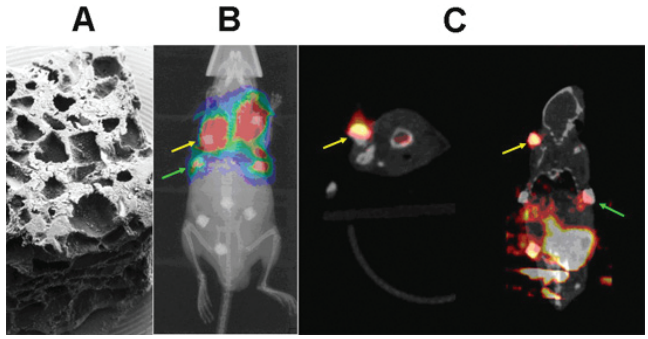

Figure 6. Imaging cube implants using the triple fusion reporter. (A) ceramic cube for cell loading and implant; (B) BLI of 8-cube implants: top row (yellow arrow) loaded with transduced hMSCs, second row (green arrow) loaded with a mixture of wt and transduced hMSCs, and the rest with either vector-transduced or being empty; (C) overlays of PET (hot metal) and CT (grey scale) images: transaxial (left) and coronal (right) views, in which the cubes were also visible on the CT images. While top-row cubes (yellow arrows) had strong PET signals, the second row cubes (green arrow) loaded with a mixture of wt and transduced hMSCs were visible despite of dilution. High and nonspecific uptake of FHBG in the gut is due mainly to FHBG's lipophilicity.

cells and therefore do not reject human cells, and have been successfully used to test engraftment of human hematopoietic cells (58). All animal procedures were approved by the local IACUC.

In one group, NOD-SCID mice implanted with porous, fibronectin-coated ceramic cubes (Zimmer, Inc., Warsaw, IN) loaded with NIS-transduced human MSC (total of 4 cubes, 2 cubes placed in each flank, 1 cm apart each containing different numbers of NIS-MSCs) were on the same mouse. Ceramic cubes can concentrate a range of MSCs in a physical location to enhance tracer signal and provide a microenvironment for long-term survival of MSCs in NOD-SCID mice. In a second group, NOD-SCID mice were injected subcutaneously (s.c.) with 1×10^6, 2×10^6, and 4×10^6 NIS-MSCs per mouse on different mice. This was to test the mobility of s.c.-injected MSC.

One day after cube implant, [^{99m}Tc]-TcO_4^-, a substrate for NIS, was injected through the tail vein and the NOD-SCID mice were imaged on the X-SPECT (Gamma Medica, Northridge, CA) 25–30 minutes postpertechnetate injection. During SPECT imaging, the animal was kept under isoflurane gas anesthesia maintained by the EZ-anesthesia system (Euthanex, Palmer, PA). The images were reconstructed by using an iterative algorithm available on the scanner. A CT scan was conducted immediately after the SPECT scan while the anesthetized animal remained in the same position, and was easily aligned with SPECT images as shown in Figure 5. The top three CT images are axial, sagittal, and coronal cuts of the mouse. The middle three are the same cuts from SPECT scan and bottom three panels are the pseudo-color overlay between the two. Compared with the negative controls (with blank cube implants, images not shown here), the positive controls clearly showed uptake of pertechnetate. Figure 5B shows the s.c. injection of 2×10^6 NIS-MSC (arrow). The tracer dose and imaging parameters were identical to the cube experiments. While these initial imaging results were very encouraging for identifying the positive control targets, background signals from thyroid and stomach due to endogenous NIS gene expression could potentially interfere with true targeting signals. The other issue was the loss of image signal as encountered by other investigators using the same CMV promoter to drive imaging reporter gene(s) for stem cells imaging (59, 60). We thus moved to another report gene system for labeling as discussed next.

Imaging with the Triple Fusion Reporter. This reporter system allows for longitudinal imaging, both qualitatively and quantitatively, of transplants of transduced human MSCs *in vivo* in small animal models. The triple reporter gene *fluc-mrfp-ttk* (a gift from Sam S. Gambhir, Stanford University) encodes a fusion protein containing functional components from *fluc*, monomeric red fluorescent protein (*mrfp*), and truncated HSV1 sr39tk (*ttk*), whose product can thus be visualized using BLI, fluorescent, and PET imaging, respectively (61). The three components or domains were linked by 14-amino acid (LENSHASAGY-QAST) and 8-amino acid (TAGPGSAT) segments, respectively. The *ttk* domain contains a deletion in the first 135 bp that eliminates the nuclear localization signal. As a result, higher cytosolic versus nuclear concentration brings less cytotoxicity and improved image signal. Enzymatic activity of each domain in this reporter was previously shown to be 54% for *fluc*, "medium" for *mrfp*, and 100% for *ttk*, when compared with their full-length individual counterparts. The choice of this fusion reporter with undiminished *tk* activity was based on the potential for PET imaging that would be most useful in future clinical translation. Though this and similar reporters have been used previously in the context of stem cell transplants (61–64), our study is unique in its use of a second generation lentiviral vector for reporter gene transduction, in the use of native human MSCs, and in the

thorough examination of reporter effects on stem cell phenotype. In particular, the differences between this and the other published MSC tracking study (27) are: 1) this study is a general purpose investigation on imaging-based MSC tracking technique while the other study focused on tumor metastasis tracking; 2) primary human MSCs were used here instead of immortalized MSCs; 3) this study used a triple fusion reporter (*fluc-mrfp-ttk*) instead of a dual reporter (*egfp-tk*), and the addition of *fluc* allows convenient and sensitive BLI imaging; and 4) a modified myeloproliferative sarcoma virus (MPSV) promoter or MND promoter was used to drive triple reporter expression as it has been shown to be more resistant to epigenetic silencing (65) than the promoter of EF1α or CMV.

Transduction of hMSCs at an MOI of 8 yielded a transduction efficiency of 83% as determined by *mrfp* FACS analysis. Reporter transduced human MSCs (for imaging) were loaded into the same ceramic cubes used previously as shown in Figure 6A and subcutaneously implanted into NOD-SCID mice as before. It was determined that as many as about 50K cells can be loaded into a cube by this procedure (66). To evaluate quantitative correlation of image-based measurement for estimating the number of the cells, cubes were loaded with either reporter transduced MSCs or a diluted mix of reporter transduced MSCs and empty vector-transduced MSCs. Control cubes were loaded with wild-type MSCs, empty vector-transduced MSCs, or no MSCs (empty cubes, yet another control); this allowed for intrasubject positive and negative controls. After receiving hMSCs via cube implants, mice were imaged at multiple time points for up to 3 months by BLI using the Xenogen IVIS 200 System. While still under anesthesia after BLI, the same mice were imaged by a special planar x-ray system developed jointly by Thomas Jefferson National Lab (Newport News, VA) and Case Western Reserve University (Cleveland, OH) to precisely determine cube position. BLI and planar x-ray images were aligned using Pmod (software package from Pmod Technologies, Zurich, Switzerland), which allowed semiquantitative analysis of BLI data in defined regions from the aligned x-ray images. Figure 6B shows the BLI signal 4 days after cube implant. There is a remarkable difference in the signal intensity between the diluted and undiluted cells that were transduced with the triple reporter. For the upper two cubes loaded with undiluted human MSC transduced with the reporter, a larger signal region resulted from the extensive diffusion and scattering of the visible light photons. The BLI signals were detectable beyond 3 months postimplantation, during which the BLI imaging signal intensity from the cubes fluctuated (67).

After BLI imaging, selected animals were imaged by CT and PET at different time points up to 2 months postimplantation. The anesthetized animals were scanned by microCT using the CT component of the Gamma Medica's X-SPECT scanner. After the CT scan, the animal was transported to a nearby R4 microPET scanner (Siemens/

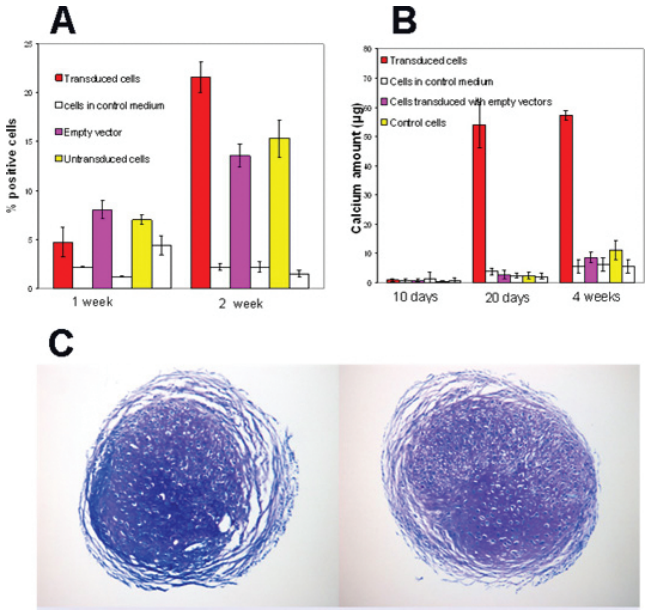

Figure 7. Retention of differentiation potentials after lenti-vector transduction of the reporter gene system. (A) adipogenic, (B) osteogenic, (C) chondrogenic assays between wt hMSCs (left) and transduced hMSCs (right).

Concord, Knoxville, TN) for PET imaging. 9-[4-[^{18}F]fluoro-3-(hydroxymethyl)butyl]guanine ([^{18}F]-FHBG), a substrate for herpes thymidine kinase (TK), was injected i.v. by tail vein, and the PET scan was performed 50 min after injection. The PET images were reconstructed using a 2-D ordered subset expectation maximization algorithm. Alignment between PET emission and CT images was done using software developed in-house. Figure 6C showed an overlay of PET slice with corresponding CT from the same animal in Figure 5 (4 days after cube implantation). The top two cubes loaded with undiluted stem cells were clearly visible, and the cube with diluted cells was also visible on the microPET scan. Regions of interest (ROI) were defined centered on cubes seen on the CT images that were aligned with the PET images. Regional data were defined as the sum of the measured radioactivity within a ROI at a specific time point. PET imaging signal from the cubes remained detectable for 2 and half months (67).

Issues with Reporter-based Imaging

Stem Cell Properties. The procedure to transduce reporter into stem cells for imaging would first ensure that the reporter system is working to provide sufficient signal for imaging. An equally important issue is whether such procedures have changed any of the proliferation and differentiation potential of the labeled stem cells. Specifically, is there any alteration to the stem cells after the transduction of the reporter gene system by way of lentiviral vector? To address this crucial issue, transduced human MSCs were compared with wild-type and empty vector-transduced MSCs to examine their ability to differ-

entiate towards adipogenic, chondrogenic, and osteogenic lineages (67).

Stem cells were induced to form adipocytes for adipogenic assay and examined using flow cytometry for the proportion of cells staining with Nile Red, a measure of cellular lipophilic content. By this method, transduced MSCs had an adipocytic phenotype similar to that in hollow lentiviral vector-transduced MSCs (vector-transduced) and untransduced MSCs (wt MSCs or untransduced MSCs) as shown in Figure 7A.

Transduced MSCs, vector-transduced MSCs, and untransduced MSCs were incubated in osteogenic medium containing 10% fetal bovine serum (FBS), dexamethasone, β-glycerophosphate, and ascorbic acid 2-phosphate for osteogenic assay. Controls were incubated without dexamethasone. Calcium was extracted and measured as a marker for osteoblastic differentiation. The osteogenic potential of transduced MSCs was preserved (Figure 7B).

For chondrogenic assay, MSCs were cultured in aggregate form in medium that contains insulin, transferrin, selenous acid, dexamethasone, sodium pyruvate, ascorbic acid 2-phosphate, and TGF-β1. The resulting pellets were fixed and stained with toluidine blue (0.2%) for visual assessment of chondrogenic potential. Figure 7C showed no obvious difference between the transduced and wild-type MSCs.

Recently, microarrays have been used to evaluate the changes in the gene expression profiles associated with the stem cell differentiation (68, 69). Although a published study has examined the effects of the transduction of same triple fusion reporter genes on the transcriptional profiles of mouse embryonic stem cells (63), no study has been performed to investigate the transduction effects on human MSCs. Therefore, the transcriptional changes associated with the reporter gene transduction process were evaluated with an oligonucleotide human microarray, and RT-PCR was used to validate the microarray results (70). Significant Analysis of Microarray (SAM) identified 87 upregulated and 69 downregulated genes, respectively, with high accuracy. Annotation analysis showed that genes involved with development (FOXG1B), lipid metabolism (PTGDS), immune response (IL-8), ubiquitin cycle (UBE2D3), cell adhesion (PCDHB10), cytoskeleton organization/biogenesis (COL15A1), etc., were differentially expressed. Furthermore, some anti-apoptosis (SERPINB2, TNFAIP3) and apoptosis (PMAIP1) genes were upregulated. Genes associated with cell growth or cycles are either upregulated (DCBLD2, FGF5, ESM1; E2F7, CKS2, CDC42) or downregulated (IGF2, FGF7, IGF1; CDKN2A, CDKN2B, CDKN1C). Other genes, such as HMGA2C, which is associated with adiopogenesis, and MSC differentiation were upregulated, while LEPR (a gene related to adipocytes), MGP, PTGER4 (regulation of ossification), COMP (a cartilage-related gene) were downregulated. Despite these changes, the expression of the reporter had no significantly adverse effect on the viability, proliferation, and differentiation of MSCs as the main genes with MSC characteristics pertaining to Adipose (Leptin, Adipose diff-related factor, C/EBP α and β), Bone (Osteonectin, osf2, Cbfa-1), Cartilage (Jagged 2, Biglycan, Fibromodulin, Decorin, Aggrecan), Endo/Epithelial (VEGF, LDL Recepoter), Muscle (Cardiac Specific ATPase, Actin, gamma 2, Calreticulin, Capping protein, Z-line), Neural (TrkA Receptor, TrkB Receptor, Calretini, Neurotrophin 5), Stromal Support (SCF, SDF, M-CSF, Flt-3 ligand, IL-6), and others (MHC I, MHC II) were not altered by the reporter gene transduction process. Validation assays demonstrated the retention of the potentials of reporter-transduced MSCs for osteogenic, chondrogenic, and adipogenic differentiations.

Quantitative Issues. Using reporter gene-based approach or direct labeling for imaging, the fundamental questions for quantitative stem cell tracking are how to accurately estimate the number of cells from the image data; how sensitive are the imaging results and what is the smallest number of the cells that can be detected; and how precise the localization of the cells can be *in vivo*. Usually, it requires a series of calculations and calibrations to convert detected photon counts on the image to the number of the viable stem cells at a site or organ of interest (or an ROI on an image). Previously published data, mostly from using tumor cells, on the sensitivity of similar type of microPET scanner for detecting TK-expressing cells using the same [^{18}F]-FHBG tracer revealed a lower threshold of microPET detection at a cell density of about 1.0 million/mL (27, 71). The cubes loaded with transduced MSCs had the cell density above this lower threshold of microPET detection were clearly imaged as shown in Figure 6C, and cell density in the diluted cubes that were also detectable on microPET imaging (Figure 6C) was only about one third of the reported lower threshold. Human MSCs are larger than other cell types, such as the tumor cells used to derive the lower limits of detection, which might contribute to the greater detection sensitivity from our study. The absolute number of the transduced human MSCs giving detectable PET imaging signals in one spot (such a cube) was estimated to be around 5,000–10,000 (67).

The factors involved in quantification are equilibrium (quasi steady state) of tracer uptake, concentration of reporter gene tagged the cells, biological half lives of the tracer, etc. We are in the process of setting up a math model to aid quantitative analysis of the sequentially or dynamically acquired image data to account for stem cell proliferation, differentiation, and apoptosis at different stages of the cell life span.

Finally, due to the limitation of spatial resolution and sensitivity of the current BLI, microPET, or microSPECT systems, precise localization of single cells or stem cell niche in animal models remains difficult. We are developing a cryo-macrotome with microscopic fluorescent and potentially β particle (from C-14, H-3 decay) detection

capabilities, which would allow single cell detection during whole body slicing of a rodent.

New Developments and Future Efforts

Currently, strong promoters such as CMV, MND, etc., are used to drive constitutive expression of the reporters such as NIS, *fluc*, GFP, or dual-, tri-fusion reporter genes. Stem cells tagged with such a reporter system will light up like beacons, which would allow longitudinal monitoring of their distribution and dynamics. However, when stem cells differentiate into other lineages, such an event would not be distinguished from the image signal of undifferentiated cells. Our attention has been shifted to event- or location-specific promoters that will turned on when a specific event/function occurs or the infused stem cells arrive at a specific site or organ. One example was to use cardiac specific promoter α-Myosin Heavy Chain (α-MHC) to detect cell differentiation into cardiac myocytes (72). We have constructed vectors with TIE-1 promoter, which is endothelial specific, to drive reporter expression for imaging angiogenesis. Stem cells transduced with such vectors can be tracked for their action in repair/regeneration, or for their role in tumor metastasis. We have also constructed vectors containing collagen α1 type I promoter (Col2.3) specifically for osteogenic differentiation (73). Stem cells transduced with such vectors can be followed to assess their repair function in a bone fracture model.

So far, all imaging methods are developed to label the cells before transplant or implant. To track endogenous stem cells' activation, recruitment, homing, and engraftment, or other functions, the logical thinking is to develop specific ligand(s) to target corresponding markers on the surface of these cells. The problem with this kind of approach is that stem cells usually lack specific surface markers (74). An example will be Chemokine (C-X-C motif) receptor 4 (CXCR-4). Homing and engraftment of HSC are directed in part by stromal cell–derived factor-1α (SDF-1) and CXCR-4 (specific for SDF-1) pair, the so-called SDF-1/CXCR-4 axis (75, 76). SDF-1 and its receptor CXCR-4 were shown to be critical in human stem cell engraftment and repopulation in NOD-SCID mice (77). However, CXCR-4 expression has been documented on mature blood cells, including lymphocytes, monocytes, megakaryocytes, and platelets. It has also been detected on $CD34^+$ progenitors purified from bone marrow, mobilized peripheral blood and cord blood, and is NOT specific for HSCs. In addition, many of the stem cell surface phenotypes are variable depending on the microenvironments that the cells are exposed. Other functional markers are transient in response to the stimuli. For example, the c-Met receptor is induced by HGF and hypoxia (78). Finding targetable marker candidates for imaging endogenous stem cells and their functional behaviors remains a challenge.

We thank a group of contributors (listed in alphabetic order) who participated in various experiments or stages of the studies: Amad Awadallah, Yunhui Kim, Dr. Omer Koç, Jeffrey Kolthammer, Yu Kuang, Yuan Lin, Zachary Love, Basabi Maitra, Dr. Stan Majewski, Joseph Molter, Nicolas Salem, Dr. Luis A. Solchaga, Fangjing Wang, and Dr. Andrew Wiesenberger.

1. Bertz H, Illerhaus G, Veelken H, Finke J. Allogeneic hematopoietic stem-cell transplantation for patients with relapsed or refractory lymphomas: comparison of high-dose conventional conditioning versus fludarabine-based reduced-intensity regimens. Ann Oncol 13:135–139, 2002.
2. Gratwohl A, Baldomero H, Demirer T, Rosti G, Dini G, Ladenstein R, Urbano-Ispizua A. Hematopoetic stem cell transplantation for solid tumors in Europe. Ann Oncol 15:653–660, 2004.
3. Haynesworth S, Goshima J, Goldberg V, Caplan A. Characterization of cells with osteogenic potential from human marrow. Bone 13:81–88, 1992.
4. Pittinger M, Mackay A, Beck S, Jaiswal R, Douglas R, Mosca J, Moorman M, Simonetti D, Craig S, Marshak D. Multilineage potential of adult human mesenchymal stem cells. Science 284:143–147, 1999.
5. Caplan A. Mesenchymal stem cells. J Orthop Res 9:641–650, 1991.
6. Devine SM, Cobbs C, Jennings M, Bartholomew A, Hoffman R. Mesenchymal stem cells distribute to a wide range of tissues following systemic infusion into nonhuman primates. Blood 101:2999–3001, 2003.
7. Koc ON, Gerson SL, Cooper BW, Dyhouse SM, Haynesworth SE, Caplan AI, Lazarus HM. Rapid hematopoietic recovery after coinfusion of autologous-blood stem cells and culture-expanded marrow mesenchymal stem cells in advanced breast cancer patients receiving high-dose chemotherapy. J Clin Oncol 18:307–316, 2000.
8. Lazarus HM, Koc ON, Devine SM, Curtin P, Maziarz RT, Holland HK, Shpall EJ, McCarthy P, Atkinson K, Cooper BW, Gerson SL, Laughlin MJ, Loberiza FR Jr, Moseley AB, Bacigalupo A. Cotransplantation of HLA-identical sibling culture-expanded mesenchymal stem cells and hematopoietic stem cells in hematologic malignancy patients. Biol Blood Marrow Transplant 11:389–398, 2005.
9. Le Blanc K, Rasmusson I, Sundberg B, Gotherstrom C, Hassan M, Uzunel M, Ringden O. Treatment of severe acute graft-versus-host disease with third party haploidentical mesenchymal stem cells. Lancet 363:1439–1441, 2004.
10. Nakamizo A, Marini F, Amano T, Khan A, Studeny M, Gumin J, Chen J, Hentschel S, Vecil G, Dembinski J, Andreeff M, Lang FF. Human bone marrow-derived mesenchymal stem cells in the treatment of gliomas. Cancer Res 65:3307–3318, 2005.
11. Daley GQ, Goodell MA, Snyder EY. Realistic prospects for stem cell therapeutics. Hematol Am Soc Hematol Educ Program 398–418, 2003.
12. Li Y, Chen J, Chen XG, Wang L, Gautam SC, Xu YX, Katakowski M, Zhang LJ, Lu M, Janakiraman N, Chopp M. Human marrow stromal cell therapy for stroke in rat: neurotrophins and functional recovery. Neurology 59:514–523, 2002.
13. Arbab AS, Yocum GT, Kalish H, Jordan EK, Anderson SA, Khakoo AY, Read EJ, Frank JA. Efficient magnetic cell labeling with protamine sulfate complexed to ferumoxides for cellular MRI. Blood 104:1217–23, 2004.
14. Bulte JW, Arbab AS, Douglas T, Frank JA. Preparation of magnetically labeled cells for cell tracking by magnetic resonance imaging. Methods Enzymol 386:275–299, 2004.
15. Partlow KC, Chen J, Brant JA, Neubauer AM, Meyerrose TE, Creer MH, Nolta JA, Caruthers SD, Lanza GM, Wickline SA. 19F magnetic resonance imaging for stem/progenitor cell tracking with multiple unique perfluorocarbon nanobeacons. Faseb J 21:1647–1654, 2007.
16. Hofmann M, Wollert KC, Meyer GP, Menke A, Arseniev L, Hertenstein B, Ganser A, Knapp WH, Drexler H. Monitoring of bone marrow cell homing into the infarcted human myocardium. Circulation 111:2198–2202, 2005.

17. Ma B, Hankenson KD, Dennis JE, Caplan AI, Goldstein SA, Kilbourn MR. A simple method for stem cell labeling with fluorine 18. Nucl Med Biol 32:701–705, 2005.
18. Bindslev L, Haack-Sorensen M, Bisgaard K, Kragh L, Mortensen S, Hesse B, Kjaer A, Kastrup J. Labelling of human mesenchymal stem cells with indium-111 for SPECT imaging: effect on cell proliferation and differentiation. Eur J Nucl Med Mol Imaging, 2006.
19. Gao J, Dennis JE, Muzic RF, Lundberg M, Caplan AI. The dynamic in vivo distribution of bone marrow-derived mesenchymal stem cells after infusion. Cells Tissues Organs 169:12–20, 2001.
20. Jin Y, Kong H, Stodilka RZ, Wells RG, Zabel P, Merrifield PA, Sykes J, Prato FS. Determining the minimum number of detectable cardiac-transplanted 111In-tropolone-labelled bone-marrow-derived mesenchymal stem cells by SPECT. Phys Med Biol 50:4445–4455, 2005.
21. Brenner W, Aicher A, Eckey T, Massoudi S, Zuhayra M, Koehl U, Heeschen C, Kampen WU, Zeiher AM, Dimmeler S, Henze E. 111In-labeled CD34+ hematopoietic progenitor cells in a rat myocardial infarction model. J Nucl Med 45:512–518, 2004.
22. Aicher A, Brenner W, Zuhayra M, Badorff C, Massoudi S, Assmus B, Eckey T, Henze E, Zeiher AM, Dimmeler S. Assessment of the tissue distribution of transplanted human endothelial progenitor cells by radioactive labeling. Circulation 107:2134–2139, 2003.
23. Bettin K, Allen MO, Gerding DN, Forstrom L, Shafer R. In-111 Pseudomonas aeruginosa: a simple method of labeling live bacteria with a gamma-emitting radioisotope. Eur J Nucl Med 12:277–279, 1986.
24. Mangi A, Noiseux N, Kong D, He H, Rezvani M, Ingwall J, Dzau V. Mesenchymal stem cells genetically modified with AKT prevent remodeling and restore performance of infarcted hearts. Nature Med 9: 1195–1201, 2003.
25. Min JJ, Ahn Y, Moon S, Kim YS, Park JE, Kim SM, Le UN, Wu JC, Joo SY, Hong MH, Yang DH, Jeong MH, Song CH, Jeong YH, Yoo KY, Kang KS, Bom HS. In vivo bioluminescence imaging of cord blood derived mesenchymal stem cell transplantation into rat myocardium. Ann Nucl Med 20:165–170, 2006.
26. Pelled G, Tai K, Sheyn D, Zilberman Y, Kumbar S, Nair LS, Laurencin CT, Gazit D, Ortiz C. Structural and nanoindentation studies of stem cell-based tissue-engineered bone. J Biomech, 2006.
27. Hung SC, Deng WP, Yang WK, Liu RS, Lee CC, Su RC, Lin RJ, Yang DM, Chang CW, Chen WH, Wei HJ, Gelovani JG. Mesenchymal stem cell targeting of microscopic tumors and tumor stroma development monitored by noninvasive in vivo positron emission tomography imaging. Clin Cancer Res 11:7749–7756, 2005.
28. Bai JZ, Ding WM, Liu ZJ, Yu MJ, Tian JH, Wang F, Du J, Zhang XY, Li LS, Shen L. [Transferrin receptor expression of human mesenchymal stem cells and in vitro tracking by autoradiography after transplantation in spinal cord]. Beijing Da Xue Xue Bao 36:276–280, 2004.
29. van Dyke K, van Dyke C, Woodfork K. Luminescence Biotechnology: Instruments and applications. Boca Raton, FL: CRC Press, 2002.
30. Bushberg JT, Seibert JA, Leidholdt J, Boone EM, Boone JM. The Essential Physics of Medical Imaging, 2nd ed. Philadelphia, PA: Lippincott Williams & Wilkins, 2002.
31. Valk PE, Bailey DL, Townsend DW, Maisey MN. Positron Emission Tomography: Basic science and clinical practice. London: Springer-Verlag, 2003.
32. Kalish H, Arbab AS, Miller BR, Lewis BK, Zywicke HA, Bulte JW, Bryant LH Jr, Frank JA. Combination of transfection agents and magnetic resonance contrast agents for cellular imaging: relationship between relaxivities, electrostatic forces, and chemical composition. Magn Reson Med 50:275–282, 2003.
33. Walczak P, Kedziorek DA, Gilad AA, Lin S, Bulte JW. Instant MR labeling of stem cells using magnetoelectroporation. Magn Reson Med 54:769–774, 2005.
34. Zhou R, Acton PD, Ferrari VA. Imaging stem cells implanted in infarcted myocardium. J Am Coll Cardiol 48:2094–2106, 2006.
35. Lennon DP, Haynesworth SE, Bruder SP, Jaiswal N, Caplan AI. Human and animal mesenchymal progenitor cells from bone marrow: Identification of serum for optimal selection and proliferation. In Vitro Cell Dev Biol 32:602–611, 1996.
36. DeLuca M, McElroy WD. Kinetics of the firefly luciferase catalyzed reactions. Biochemistry 13:921–925, 1974.
37. Cook SH, Griffin DE. Luciferase imaging of a neurotropic viral infection in intact animals. J Virol 77:5333–5338, 2003.
38. Hardy J, Francis KP, DeBoer M, Chu P, Gibbs K, Contag CH. Extracellular replication of Listeria monocytogenes in the murine gall bladder. Science 303:851–853, 2004.
39. Luker GD, Pica CM, Song J, Luker KE, Piwnica-Worms D. Imaging 26S proteasome activity and inhibition in living mice. Nat Med 9:969–973, 2003.
40. Paulmurugan R, Umezawa Y, Gambhir SS. Noninvasive imaging of protein-protein interactions in living subjects by using reporter protein complementation and reconstitution strategies. Proc Natl Acad Sci U S A 99:15608–15613, 2002.
41. Sarraf-Yazdi S, Mi J, Dewhirst MW, Clary BM. Use of in vivo bioluminescence imaging to predict hepatic tumor burden in mice. J Surg Res 120:249–255, 2004.
42. Wetterwald A, van der Pluijm G, Que I, Sijmons B, Buijs J, Karperien M, Lowik CW, Gautschi E, Thalmann GN, Cecchini MG. Optical imaging of cancer metastasis to bone marrow: a mouse model of minimal residual disease. Am J Pathol 160:1143–1153, 2002.
43. Zhang GJ, Safran M, Wei W, Sorensen E, Lassota P, Zhelev N, Neuberg DS, Shapiro G, Kaelin WG, Jr. Bioluminescent imaging of Cdk2 inhibition in vivo. Nat Med 10:643–648, 2004.
44. Cao YA, Wagers AJ, Beilhack A, Dusich J, Bachmann MH, Negrin RS, Weissman IL, Contag CH. Shifting foci of hematopoiesis during reconstitution from single stem cells. Proc Natl Acad Sci U S A 101: 221–226, 2004.
45. Lin Y, Cheung P, Wilson DL, Gerson SJ. Visualization of enhanced clonal expansion bioluminescence imaging. Mol Imaging 3:282, 2004.
46. Jaffee EM, Dranoff G, Cohen LK, Hauda KM, Clift S, M. F. F, Mulligan RC, Pardoll DC. High efficiency gene transfer into primary human tumor explants without cell selection. Cancer Res 53:2221, 1993.
47. de Felipe P, Hughes LE, Ryan MD, Brown JD. Co-translational, intraribosomal cleavage of polypeptides by the foot-and-mouth disease virus 2A peptide. J Biol Chem 278:11441–11448, 2003.
48. Donnelly ML, Hughes LE, Luke G, Mendoza H, ten Dam R, Gani F, Ryan MF. The 'cleavage' activities of foot-and-mouth disease virus 2A site-directed mutants and naturally occurring '2A-like' sequences. J Gen Virol 82:1027–1041, 2001.
49. Davis BM, Koc ON, Gerson SL. Limiting numbers of G156A O(6)-methylguanine-DNA methyltransferase-transduced marrow progenitors repopulate nonmyeloablated mice after drug selection. Blood 95:3078–3084, 2000.
50. Chang SM, Theodosopoulos P, Lamborn K, Malec M, Rabbitt J, Page M, Prados MD. Temozolomide in the treatment of recurrent malignant glioma. Cancer 100:605–611, 2004.
51. Sawai N, Zhou S, Vanin EF, Houghton P, Brent TP, Sorrentino BP. Protection and in vivo selection of hematopoietic stem cells using temozolomide, O6-benzylguanine, and an alkyltransferase-expressing retroviral vector. Mol Ther 3:78–87, 2001.
52. Niu G, Gaut AW, Ponto LL, Hichwa RD, Madsen MT, Graham MM, Domann FE. Multimodality noninvasive imaging of gene transfer using the human sodium iodide symporter. J Nucl Med 45:445–449, 2004.
53. La Perle KM, Shen D, Buckwalter TL, Williams B, Haynam A, Hinkle G, Pozderac R, Capen CC, Jhiang SM. In vivo expression and function of the sodium iodide symporter following gene transfer in the MATLyLu rat model of metastatic prostate cancer. Prostate 50:170–178, 2002.
54. Zuckier LS, Dohan O, Li Y, Chang CJ, Carrasco N, Dadachova E.

Kinetics of perrhenate uptake and comparative biodistribution of perrhenate, pertechnetate, and iodide by NaI symporter-expressing tissues in vivo. J Nucl Med 45:500–507, 2004.

55. Chung JK. Sodium iodide symporter: its role in nuclear medicine. J Nucl Med 43:1188–1200, 2002.
56. Lee Z, Koc ON, Wojtkiewicz GR, Maitra B, Gerson SL. In vitro evaluation of imaging potential of mesenchymal stem cell transplant following NIS transfer. Mol Imaging 2:284, 2003.
57. Lee Z, Koc ON, Wojtkiewicz GR, Maitra B, Faulhaber PF, Gerson SL. Imaging mesenchymal stem cell transplant on small animal models. J Nucl Med 45:196, 2004.
58. Tournoy KG, Depraetere S, Pauwels RA, Leroux-Roels GG. Mouse strain and conditioning regimen determine survival and function of human leucocytes in immunodeficient mice. Clin Exp Immunol 119: 231–239, 2000.
59. Kim YH, Lee DS, Kang JH, Lee YJ, Chung JK, Roh JK, Kim SU, Lee MC. Reversing the silencing of reporter sodium/iodide symporter transgene for stem cell tracking. J Nucl Med 46:305–311, 2005.
60. Wu JC, Wang D, Chen IY, Park JM, Patel MR, Gheyens O, Tseng JR, Gambhir SS. Molecular mechanism of reporter gene silencing and reversal in cell transplant imaging. Mol Imaging Biol 7:107, 2005.
61. Ray P, De A, Min JJ, Tsien RY, Gambhir SS. Imaging tri-fusion multimodality reporter gene expression in living subjects. Cancer Res 64:1323–1330, 2004.
62. Cao F, Lin S, Xie X, Ray P, Patel M, Zhang X, Drukker M, Dylla SL, Connolly AJ, Chen X, Weissman IL, Gambhir SS, Wu JC. In vivo visualization of embryonic stem cell survival, proliferation, and migration after cardiac delivery. Circulation 113:1005–1014, 2006.
63. Wu JC, Spin JM, Cao F, Lin S, Xie X, Gheysens O, Chen IY, Sheikh AY, Robbins RC, Tsalenko A, Gambhir SS, Quertermous T. Transcriptional profiling of reporter genes used for molecular imaging of embryonic stem cell transplantation. Physiol Genomics 25:29–38, 2006.
64. Ponomarev V, Doubrovin M, Serganova I, Vider J, Shavrin A, Beresten T, Ivanova A, Ageyeva L, Tourkova V, Balatoni J, Bornmann W, Blasberg R, Gelovani Tjuvajev J. A novel triple-modality reporter gene for whole-body fluorescent, bioluminescent, and nuclear noninvasive imaging. Eur J Nucl Med Mol Imaging 31:740–751, 2004.
65. Krishnan M, Park JM, Cao F, Wang D, Paulmurugan R, Tseng JR, Gonzalgo ML, Gambhir SS, Wu JC. Effects of epigenetic modulation on reporter gene expression: implications for stem cell imaging. Faseb J 20:106–108, 2006.
66. Dennis JE, Haynesworth SE, Young RG, Caplan AI. Osteogenesis in marrow-derived mesenchymal cell porous ceramic composites transplanted subcutaneously: effect of fibronectin and laminin on cell retention and rate of osteogenic expression. Cell Transplant 1:23–32, 1992.
67. Love Z, Wang F, Dennis JE, Awadallah A, Salem N, Lin Y, Wiesenberger A, Majewski S, Gerson SL, Lee Z. Imaging of mesenchymal stem cell transplant by bioluminescence and PET. J Nucl Med (in press).
68. Qi H, Aguiar DJ, Williams SM, La Pean A, Pan W, Verfaillie CM. Identification of genes responsible for osteoblast differentiation from human mesodermal progenitor cells. Proc Natl Acad Sci U S A 100: 3305–3310, 2003.
69. Kalajzic I, Staal A, Yang WP, Wu Y, Johnson SE, Feyen JH, Krueger W, Maye P, Yu F, Zhao Y, Kuo L, Gupta RR, Achenie LE, Wang HW, Shin DG, Rowe DW. Expression profile of osteoblast lineage at defined stages of differentiation. J Biol Chem 280:24618–24626, 2005.
70. Wang F, Awadallah A, Solchaga LA, Kuang Y, Salem N, Lin Y, Kim YH, Love Z, Dennis JE, Gerson SL, Lee Z. Transcription profiling of reporter genes used for molecular imaging of human mesenchymal stem cells. In: Adult Mesenchymal Stem Cells in Regenerative Medicine. Cleveland, OH: 2007.
71. Su H, Forbes A, Gambhir SS, Braun J. Quantitation of cell number by a positron emission tomography reporter gene strategy. Mol Imaging Biol 6:139–148, 2004.
72. Kang JH, Lee DS, Paeng JC, Lee JS, Kim YH, Lee YJ, Hwang DW, Jeong JM, Lim SM, Chung JK, Lee MC. Development of a sodium/iodide symporter (NIS)-transgenic mouse for imaging of cardiomyocyte-specific reporter gene expression. J Nucl Med 46:479–483, 2005.
73. Kim YH, Dennis JE, Gerson SL, Lee Z. Evaluation of stem cell differentiation by in vivo imaging. Mol Imaging 6, 2007.
74. National Institutes of Health. Stem Cell Markers. U.S. Department of Health and Human Services, 2006. Available at <http://stemcells.nih.gov/info/scireport/appendixe>
75. Pituch-Noworolska A, Majka M, Janowska-Wieczorek A, Baj-Krzyworzeka M, Urbanowicz B, Malec E, Ratajczak MZ. Circulating CXCR4-positive stem/progenitor cells compete for SDF-1-positive niches in bone marrow, muscle and neural tissues: an alternative hypothesis to stem cell plasticity. Folia Histochem Cytobiol 41:13–21, 2003.
76. Ratajczak MZ, Majka M, Kucia M, Drukala J, Pietrzkowski Z, Peiper S, Janowska-Wieczorek A. Expression of functional CXCR4 by muscle satellite cells and secretion of SDF-1 by muscle-derived fibroblasts is associated with the presence of both muscle progenitors in bone marrow and hematopoietic stem/progenitor cells in muscles. Stem Cells 21:363–371, 2003.
77. Peled A, Petit I, Kollet O, Magid M, Ponomaryov T, Byk T, Nagler A, Ben-Hur H, Many A, Lapidot T. Dependence of human stem cell engraftment and repopulation of NOD/SCID mice on CXCR4. Science 283:845–848, 1999.
78. Neuss S, Becher E, Woltje M, Tietze L, Jahnen-Dechent W. Functional expression of HGF and HGF receptor/c-met in adult human mesenchymal stem cells suggests a role in cell mobilization, tissue repair, and wound healing. Stem Cells 22:405–414, 2004.